Available online at www.sciencedirect.com
ScienceDirect
Trans. Nonferrous Met. Soc. China 27(2017) 1996−2006
Transactions of Nonferrous Metals Society of China
www.tnmsc.cn

Microstructure and properties of co-continuous (β-TCP+MgO)/Zn−Mg composite fabricated by suction exsorption for biomedical applications

Xiang WANG[1], Qi-dong NIE[1], Xu-liang MA[2], Jin-long FAN[1], Ting-liang YAN[1], Xin-lin LI[1]

1. Institute of Surface/Interface Science and Technology, Key Laboratory of Superlight Material and Surface Technology, Ministry of Education, Harbin Engineering University, Harbin 150001, China;
2. School of Materials Science and Engineering, Harbin University of Science and Technology, Harbin 150080, China

Received 14 May 2016; accepted 19 September 2016

Abstract: The biomedical co-continuous (β-TCP+MgO)/Zn−Mg composite was fabricated by infiltrating Zn−Mg alloy into porous β-TCP+MgO using suction exsorption technique. The microstructure, mechanical properties and corrosion behaviors of the composite were evaluated by means of scanning electron microscopy (SEM), X-ray diffraction (XRD), mechanical testing, electrochemical and immersion test. It was found that the molten Zn−Mg alloy had infiltrated not only into the pores but also into the struts of the porous β-TCP+MgO scaffold to form a compact composite. The Zn−Mg alloy contacted to the β-TCP+MgO scaffold closely, and no reaction layer can be found between the alloy and the scaffold. The compressive strength of the composite was as high as 244 MPa, which was about 1000 times higher than that of the original porous β-TCP+MgO scaffold and 2/3 of the strength of the Zn−Mg bulk alloy. The electrochemical and immersion tests in simulated body fluid (SBF) solution indicated that the corrosion resistance of the composite was better than that of the Zn−Mg bulk alloy. The corrosion products on the composite surface were mainly $Zn(OH)_2$. Appropriate mechanical and corrosion properties indicated that the (β-TCP+MgO)/Zn−Mg composite fabricated by suction exsorption would be a very promising candidate for bone substitute.

Key words: (β-TCP+MgO)/Zn−Mg composite; microstructure; mechanical properties; corrosion behavior; suction exsorption

1 Introduction

Biodegradable materials for bone repairs have attracted much attention in the field of biomaterials due to their biodegradabilities to avoid the second surgeries and reduce the pain and economic cost for patients. Biodegradable polymers, metals and ceramics are the main three kinds of widely studied biodegradable biomaterials. At present, biodegradable polymers and ceramics are already applied in clinic and biodegradable Mg-based metals are a class of new biodegradable materials still in development [1]. Biodegradable polymers, such as poly-glycolic acid (PGA), poly-lactic acid (PLA) and poly (dl-lactide-co-glycolide) (PLGA), are the primary materials for bone repair implants. However, relatively low mechanical strength is the main disadvantage for polymers. And the acidic degradation products of polymer are possible to induce inflammation [2]. Calcium phosphates (CaPs) ceramics are the most widely used bone substitutes in bone tissue engineering due to their compositional similarities to bone mineral and excellent biocompatibility. In recent years, CaPs, especially hydroxyapatite and tricalcium phosphate, have attracted significant interest as bone substitute [3]. However, the low strength and brittleness of CaPs ceramics limit their clinical application [4]. Mg and Zn have been reported to influence osteoblast and osteoclast activity. Compared with other metallic or polymer implant materials, Mg alloys show a good combination of biocompatibility and mechanical properties, which makes them a promising materials for the production of biodegradable bone implant in osteosynthesis [5−7]. Many Mg alloys, such as Mg−Ca [8], Mg−Zn [9], Mg−Zn−Mn [10], Mg−Y [11], AZ91 and AZ31 alloys [12], have been studied. However, the rapid degradation rate of Mg alloys in human bio-environment limits their clinical applications [13]. Even worse, the evolved hydrogen bubbles from a corroding Mg implant will delay healing of the surgery

Foundation item: Project (51101039) supported by the National Natural Science Foundation of China; Project (E201005) supported by the Natural Science Foundation of Heilongjiang Province, China
Corresponding author: Xiang WANG; Tel: +86-451-82589600; E-mail: wangxiang@hrbeu.edu.cn
DOI: 10.1016/S1003-6326(17)60224-3

region and lead to necrosis of tissues [14]. The main advantage of Zn alloys over Mg alloys lies in their significantly better corrosion resistance in simulated body fluid (SBF). The low corrosion rate results in low rates of pH value increase and hydrogen evolution. Both factors are very important to prevent negative reactions in tissue during healing [15,16]. Zn has a dual role in promoting bone formation by promoting osteoblast differentiation and activity whilst simultaneously suppressing osteoclastogenesis and resorption [17−19]. VOJTĚCH et al [15] found that the Zn−Mg alloys, particularly the Zn−1%Mg alloy, comparing the strength and plasticity of Mg and Zn, achieved stronger mechanical properties. The corrosion rates of the Zn−Mg alloys were significantly lower than those of Mg and AZ91HP alloys. In addition, the possible doses of Zn ions released from implants are significantly less than Zn tolerable limit. However, the pharmacological performance of Zn ions is dependent on the release behavior. Generally, the initial burst release of ions in the body may induce adverse reactions. Thus, the release process should be controlled, and a slow and sustained rate is required during bone tissue regeneration [20]. Meanwhile, the biocompatibility of the pure Zn and Zn alloys should be improved further. In order to improve the release behavior of Zn alloys, many investigations have been done recently. LUO et al [16] prepared Zn-containing β-tricalcium phosphate (Zn-TCP), and found that Zn-TCP enhanced osteogenic differentiation of human bone marrow stromall cells (hBMSC) and regulated osteoclastic differentiation of monocyte/ macrophages in vitro. ZOU et al [21] also prepared cytocompatible and magnetic Zn−ferrite nanorods via peptide-assisted process successfully. The results of cell tests showed that Zn−ferrite nanorods had little toxicity against E. *coli*, S. *aureus*, L929, and PC12 cells. MIAO et al [20] prepared a biphasic layer with a Zn-TCP phase and a fluoridated hydroxyapatite (FHA) phase on titanium alloy substrate using the sol−gel method. The results showed that Zn release behavior of Zn-TCP/FHA layer was slow without showing any of the initial "burst" release characteristics. So, the promising improving method for the release ability of Zn alloys is to fabricate composite, which is reinforced by bioceramic of natural human bone compositions such as hydroxylapatite (HA) and β-tricalcium phosphate (β-TCP). HA and β-TCP are most widely used as reinforcement of biocomposite due to their excellent biocompatibility, bioactivity and osteoconduction characteristics, as well as their chemical and crystallographic structure approaching to that of the natural bone mineral [22−24]. In addition, some studies showed that magnesium oxide (MgO) could be added as a phase stabilizer suppressing β to α phase transition to fabricate the β-TCP foam that mimics the fully interconnected porous structure, and the biodegradation of porous scaffolds could also be controlled by adjusting the amount of MgO in the β-TCP ceramics [25,26].

Among the techniques currently available for processing metal matrix composites, the properties of the composites fabricated by liquid metal infiltration technique can be adjusted by free selection of different porous scaffolds as well as the molten metals [27,28]. MIAO et al [29] fabricated the biocomposites consisting of three interpenetrating networks of TCP, HA and PLGA. The main advantages of these composites are the improved mechanical properties and the adjustable biodegradation rates for bone tissue ingrowth. In our previous study, (HA+β-TCP)/Mg−5Sn [30], β-TCP/ Mg−Zn−Mn [31] and β-TCP/MgCa [32] interpenetrating biomedical composites were also fabricated successfully by using suction casting technique. When the alloy was infiltrated into the porous scaffold, its mechanical properties were greatly improved due to the reduced porosity and the enhanced interfacial bonding. The immersion tests also indicated that the corrosion resistances of the composites were better than those of the bulk alloys. However, few attempts have been made so far to prepare (β-TCP+MgO)/Zn−Mg composites to develop a new biomedical material.

In this work, we selected Zn−Mg alloy as the matrix material and porous β-TCP+MgO as the reinforcement to prepare co-continuous (β-TCP+MgO)/Zn−Mg composite. Firstly, an interconnected porous β-TCP+ MgO scaffold was prepared by replicating the porous structure of a thermoplastic polyurethane (PU) foam, then the molten Zn−Mg alloy was infiltrated into the porous scaffold using a self-made suction exsorption equipment to fabricate the co-continuous (β-TCP+MgO)/ Zn−Mg composite. Finally, the microstructure, mechanical properties and corrosion behaviors of the resultant composite were investigated to assess its feasibility as bone tissue implant materials.

2 Experimental

2.1 Materials preparation

The fabrication of the (β-TCP+MgO)/Zn−Mg composite consists of two steps: preparation of porous β-TCP+MgO scaffold and suction exsorption of Zn−1%Mg alloy (named Zn−Mg alloy) into the scaffold. In the preparation of the porous β-TCP+MgO, a commercial thermoplastic polyurethane (PU) foam was used as a template, and the pretreatment of PU foams and adhesion of ceramic slurry were described in Ref. [33]. The ceramic slurry was prepared by mixing 50 g ceramic powder, 10 g dispersant (polyethylene glycol) and 12.5 g surfactant (polyvinyl alcohol) with 200 mL distilled water in thermostatic waterbath at 90 °C. The ceramic

powder was the mixture of β-TCP powder (average particle size of 2.5 μm) and MgO powder (average particle size of 2 μm), and the mass fraction of MgO was 1.5%. The ceramic slurry-coated PU foams were dried at 60 °C for at least 24 h in a drying oven. Then, they were heated to 600 °C with a heating rate of 0.6 °C/min for pyrolysis of the PU foam in a furnace followed by heat treating at 1100 °C for 4 h to create porous β-TCP+MgO. Subsequently, the furnace was cooled down to room temperature at a cooling rate of 5 °C/min. The porous β-TCP+MgO scaffold was weighed and kept in a desiccator.

The co-continuous (β-TCP+MgO)/Zn−Mg composite was prepared by infiltrating the molten Zn−Mg alloy into the porous β-TCP+MgO scaffold using a self-made vacuum suction exsorption equipment, and the diagram of experimental equipment is shown in Fig. 1. Firstly, the porous β-TCP+MgO scaffold was positioned in the suction exsorption equipment, which was pre-pumped from −0.08 to −0.06 MPa. A certain quantity of commercial pure Zn and Mg were melted in a resistance furnace to prepare the molten Zn−Mg alloy with a temperature of 510−530 °C. Then, the molten Zn−Mg alloy was poured into the β-TCP+MgO scaffold and the infiltration of the liquid metal into the scaffold was driven by the vacuum. During the infiltration process the pressure from −0.08 to −0.06 MPa was maintained for about 4 min until the melt solidified completely. Finally, the pressure was released and the (β-TCP+MgO)/Zn−Mg composite was removed from the suction exsorption equipment.

2.2 Microstructure characterization

The microstructures of the porous β-TCP+MgO and the co-continuous (β-TCP+MgO)/Zn−Mg composite were investigated by scanning electron microscopy (SEM) with energy dispersion spectrometry (EDS). X-ray diffraction (XRD) analysis using the Cu K_α radiation was employed to identify the constituent phases of the Zn−Mg bulk alloy and the (β-TCP+MgO)/Zn−Mg composite and their corrosion products at a step size of 0.02° with a scanning speed of 2 (°)/min.

2.3 Compressive test

Compressive test was carried out at a constant nominal strain rate of 7×10^{-4} s^{-1} on an Instron 3365 testing machine and the compressive samples were machined into rectangle solid with dimensions of 3 mm × 3 mm × 6 mm. Five identical samples were used for the compressive tests.

2.4 Electrochemical measurement

The corrosion resistance of Zn−Mg bulk alloy and the (β-TCP+MgO)/Zn−Mg composite in SBF at (37±0.5) °C was evaluated by the potentiodynamic polarization test using electrochemical workstation (SI1287). The electrochemical test was conducted using a traditional three-electrode cell with a saturated calomel electrode (SCE) as the reference, a platinum foil as the counter electrode, and the specimen with an area of 1 cm^2 as the working electrode. The polarization scan rate was controlled at 1 mV/s. The fabrication process and composition of standard SBF solution were referred to Ref. [34]. Three samples were employed for each group.

2.5 Immersion test

The immersion test was carried out according to ASTM-G31−72 standard [35]. The test samples with sizes of 5 mm × 5 mm × 8 mm were immersed in SBF at (37±0.5) °C. After different immersion periods, the samples were removed from SBF, gently rinsed with distilled water and dried at room temperature. The phase composition was analyzed using XRD. Surface microstructures of the corroded samples being cleaned using chromic acid (CrO_3) solution were observed by SEM. The pH meter (E−900, luosu, Shanghai, China)

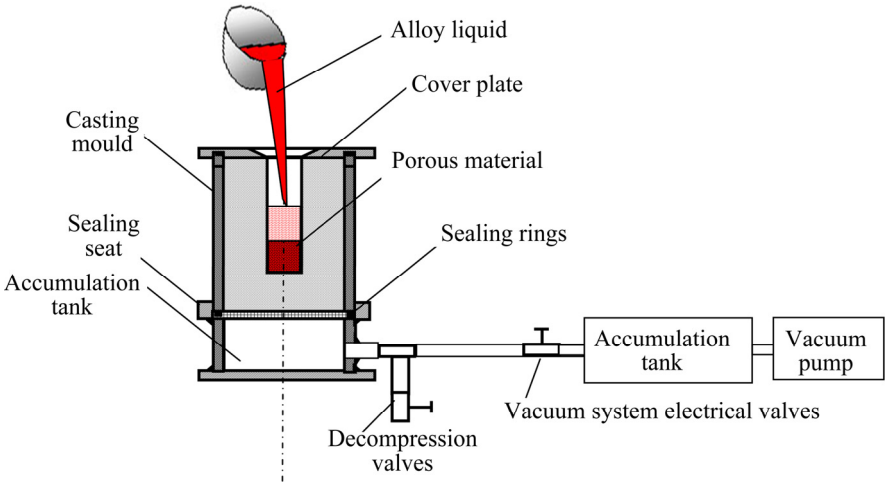

Fig. 1 Diagram of experimental equipment of suction exsorption

was used to record the change of pH value of the SBF solution during the soaking experiment. The Zn^{2+} ion concentrations in the immersion solutions were determined using inductively coupled plasma atomic emission spectrometry (5300 DV, profile ICP−AES). An average of three measurements was taken for each group.

3 Results

3.1 Microstructures and mechanical properties

The microstructure of the porous β-TCP+MgO scaffold fabricated by replicating the porous structure of PU foam is shown in Fig. 2(a). It revealed that the porous β-TCP+MgO scaffold had a fully interconnected structure, with open pores ranging from 400 to 600 μm and struts approximately 90 μm in average diameter, which provided paths for molten metal to infiltrate in and throughout the whole porous structure. It was evident that some hollow structures were formed due to the burn out of PU sponge during the pyrolysis process. In addition, no other crack-like defects appeared in the junction area of the porous cell. The average porosity of the scaffold was determined using the method in Ref. [30] to be approximately 90%.

The SEM image of the resultant co-continuous (β-TCP+MgO)/Zn−Mg composite is shown in Fig. 2(b). The dark and the gray regions corresponded to β-TCP+MgO scaffold and Zn−Mg alloy, respectively. It can be seen that the porous scaffold was filled with Zn−Mg alloy, and no pores or voids were visible in the alloy or at the Zn−Mg/β-TCP+MgO interface, which indicated good bonding between the Zn−Mg alloy and β-TCP+MgO scaffold. Meanwhile, the co-continuous networks were evident. SEM images of the interface between β-TCP+MgO scaffold and Zn−Mg alloy and EDS maps for Zn, Mg, Ca, P and O elements are shown in Fig. 3. It can be seen from Fig. 3(a) that the interfacial bonding was good, no obvious gap and discernible

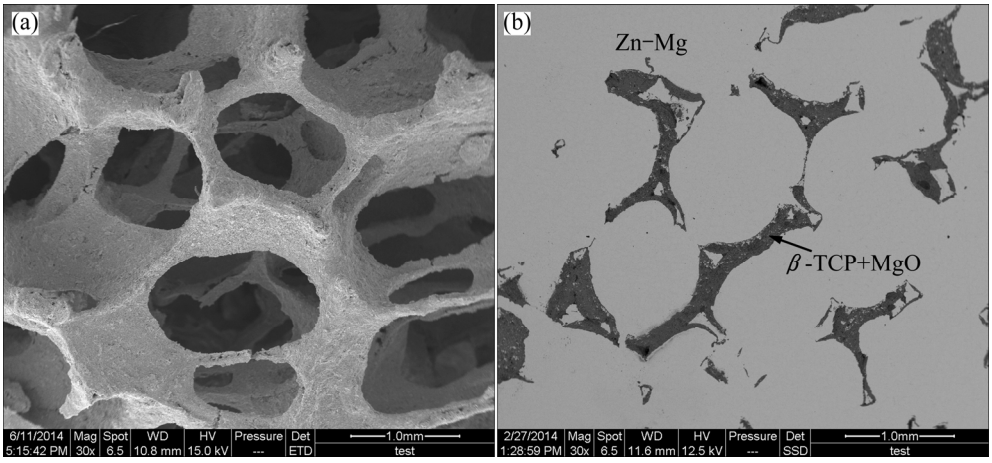

Fig. 2 SEM images of porous β-TCP+MgO (a) and (β-TCP+MgO)/Zn−Mg composite (b)

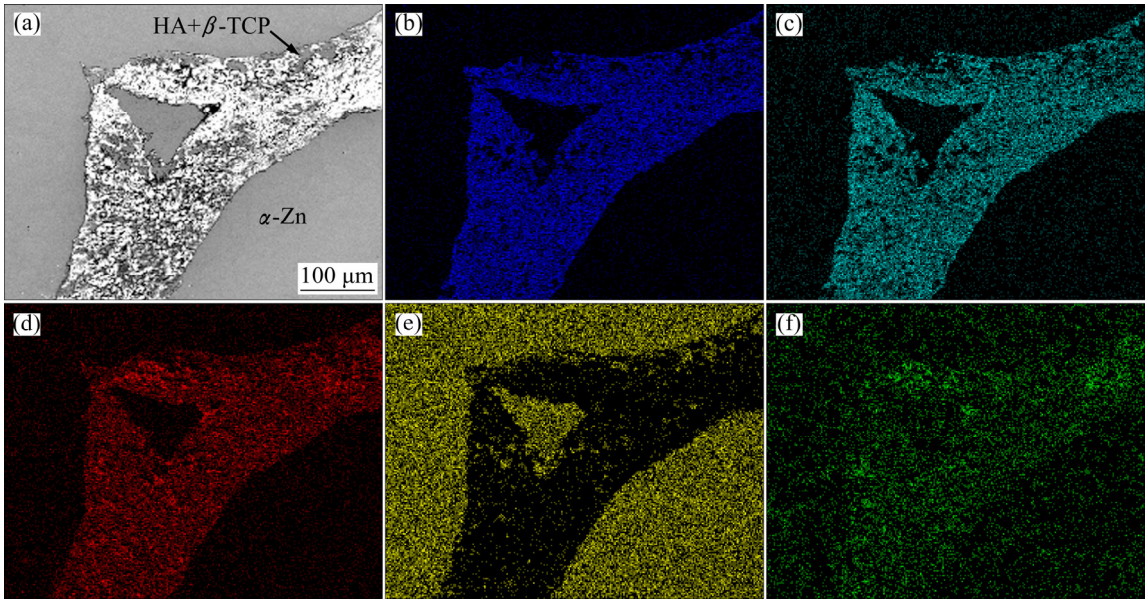

Fig. 3 SEM image of interface between β-TCP+MgO scaffold and Zn−Mg alloy (a) with EDS maps for Ca (b), P (c), O (d), Zn (e) and Mg (f) elements

debonding or reaction layer could be found at the interface between Zn−Mg alloy and β-TCP+MgO. Generally, the ceramic phase and the Zn−Mg alloy can be distinguished in Figs. 3(b)−(d), in which the ceramic phase revealed the highest Ca, P and O concentrations, and the metal phase revealed the lowest Ca, P and O concentrations. And Zn and Mg elements were observed everywhere, as shown in Figs. 3(e) and (f), revealing that the molten Zn−Mg alloy penetrated into the hollow location, the pores and the struts of the β-TCP+MgO scaffold.

Figure 4 shows the XRD patterns of the Zn−Mg alloy and the (β-TCP+MgO)/Zn−Mg composite. Compared with the Zn−Mg bulk alloy, in addition to α-Zn and Mg_2Zn_{11} phases, β-TCP and MgO phases were also identified in the (β-TCP+MgO)/Zn−Mg composite. Meanwhile, the result of the XRD analysis also demonstrated that no other phases were formed due to the reaction between the Zn−Mg alloy and β-TCP+MgO scaffold. According to Ref. [36], when Zn−Mg liquid containing 1% Mg cooled down to about 410 °C, α-Zn phase precipitated from the liquid firstly, and then Mg_2Zn_{11} intermetallic compound appeared at 364 °C. Thus, eutectics containing α-Zn and Mg_2Zn_{11} formed along the grain boundaries of Zn−Mg alloy.

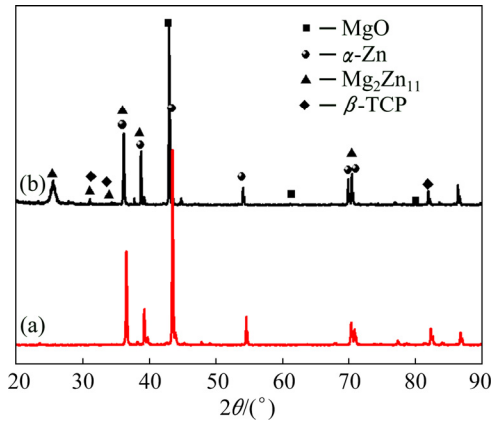

Fig. 4 XRD patterns of Zn−Mg alloy (a) and (β-TCP+MgO)/Zn−Mg composite (b)

Figure 5 shows the representative compression stress−strain curves of the (β-TCP+MgO)/Zn−Mg composite, with Zn−Mg alloy as the control. The average compressive strength of the composite was 244 MPa, which was about 1000 times higher than that of the original porous β-TCP+MgO scaffold (as shown in the inset in Fig. 5) and was approximately 2/3 of the strength of the Zn−Mg bulk alloy. The compressive strength was close to that of the natural bone (2−180 MPa).

3.2 Electrochemical measurement

Figure 6 shows the representative potentiodynamic polarization curves of the (β-TCP+MgO)/Zn−Mg composite and Zn−Mg bulk alloy at (37±0.5) °C in SBF. The corrosion potentials for the (β-TCP+MgO)/Zn−Mg composite measured in SBF were higher than those for the Zn−Mg alloy by about 0.02 V. The Zn−Mg bulk alloy exhibited a corrosion current density of 8.85 μA/cm^2 with an associated corrosion potential of −1.07 V. Compared with the Zn−Mg alloy, the corrosion potential of the (β-TCP+MgO)/Zn−Mg composite was more positive slightly, shifting to −1.05 V. Meanwhile, the corrosion current density of the (β-TCP+MgO)/Zn−Mg composite (5.12 μA/cm^2) was also lower than that of the Zn−Mg alloy. It can be inferred from the above results that the corrosion resistance of the composite was slightly better than that of the Zn−Mg bulk alloy.

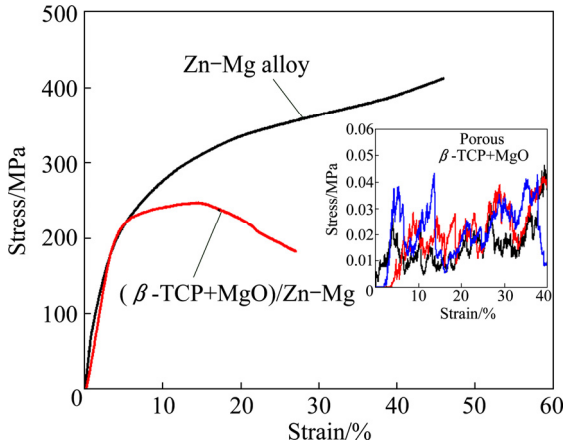

Fig. 5 Compressive behaviors of (β-TCP+MgO)/Zn−Mg composite and Zn−Mg alloy samples

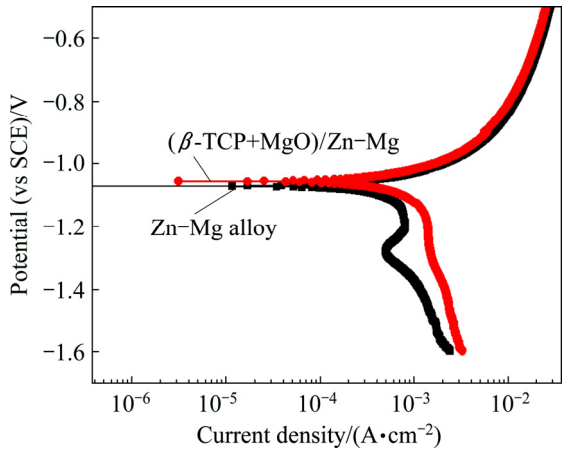

Fig. 6 Potentiodynamic polarization curves of (β-TCP+MgO)/Zn−Mg composite and Zn−Mg alloy in SBF

3.3 Immersion tests

The pH variation of the SBF solution incubating the Zn−Mg bulk alloy and (β-TCP+MgO)/Zn−Mg composite as a function of immersion time was shown in Fig. 7, with pure SBF without incubating alloy or composite as the control. It can be seen that the pH values of the SBF

incubating the Zn−Mg bulk alloy and (*β*-TCP+MgO)/Zn−Mg composite had similar change tendency with the immersion duration. In the whole process of immersion, the pH values were higher for the alloy and composite than those for pure SBF solution, but the increasing amplitude was no more than 0.4. At the first day of immersion, the pH value for the composite increased, from original 7.4 jumped to 7.8, and then the pH value decreased slowly and stabilized at about 7.3 after further immersion up to 18 d and decreased no more.

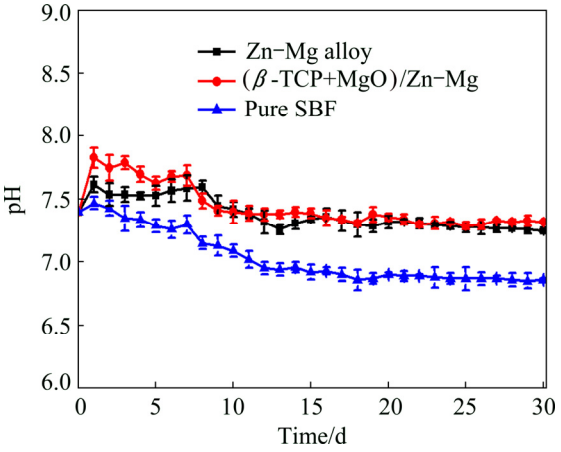

Fig. 7 pH values of SBF solution incubating (*β*-TCP+MgO)/Zn−Mg composite and Zn−Mg alloy at different immersion time

Figure 8 presents the released Zn^{2+} ion concentration from the Zn−Mg bulk alloy and the (*β*-TCP+MgO)/Zn−Mg composite in the SBF solution after 3, 7 and 15 d of immersion. It can be seen that for both the composite and the bulk alloy, the released Zn^{2+} ion concentrations increased with the increase of immersion time. After the first 3 days of immersion, the released ion concentration of the composite was higher than that of the Zn−Mg alloy. But during further immersion, the Zn^{2+} ion concentration released from the composite was lower than that from the Zn−Mg alloy instead. Furthermore, compared with the pure SBF solution, the released ion concentrations from the composite and bulk alloy were far lower than human zinc requirement of 15 mg/d [37].

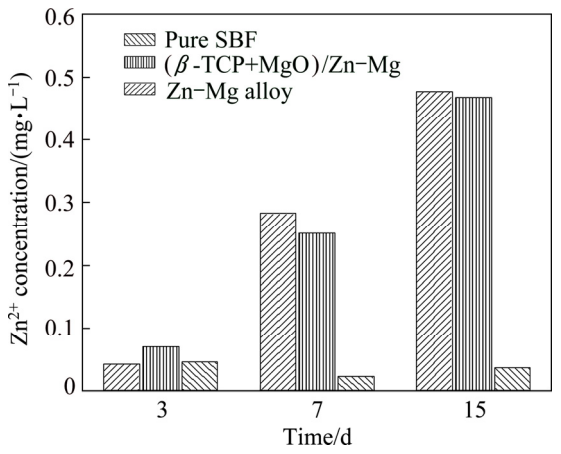

Fig. 8 Zn^{2+} concentration of SBF solutions after immersion of (*β*-TCP+MgO)/Zn−Mg composite and Zn−Mg alloy for 3, 7 and 15 d

Figure 9 illustrates the morphologies of the (*β*-TCP+MgO)/Zn−Mg composite after 3, 15 and 30 d of immersion in SBF solution at (37±0.5) °C, respectively. For the (*β*-TCP+MgO)/Zn−Mg composite, after 3 d of immersion, it exhibited rugged surface, revealing the degradation of Zn−Mg alloy, with the scaffold structure still maintaining its geometrical shape, which indicated that the degradation rate of Zn−Mg matrix alloy was quicker than that of the porous scaffold (Fig. 9(a)). After 15 d of immersion, the corrosion of the Zn−Mg matrix alloy and scaffold was also not serious, and the scaffold structures were still clear (Fig. 9(b)). The corrosion of the Zn−Mg matrix alloy and scaffolds was aggravated after 30 d of immersion, slight crevice corrosion along the interface between aggravated alloy and the scaffold was also found. But the interfacial combination between the Zn−Mg matrix alloy and scaffold was still very good (Figs. 9(c) and (d)). XRD results revealed that the main corrosion product on the composite surface was mainly zinc hydroxide ($Zn(OH)_2$), as shown in Fig. 10.

4 Discussion

Compared with the microstructure of porous *β*-TCP+MgO, it can be found that the (*β*-TCP+MgO)/Zn−Mg composite had a closed-cell and compact structure, and the interface between Zn−Mg alloy and *β*-TCP+MgO scaffold was good without discernible debonding or micro-crack. The microstructure of the co-continuous (*β*-TCP+MgO)/Zn−Mg composite indicated that the molten Zn−Mg alloy infiltrated not only into the pore but also into the struts of the *β*-TCP+MgO scaffold. This compact structure also demonstrated the efficient infiltration of the Zn−Mg alloy throughout the porous scaffold. In addition, our previous study about interpenetrating composites [31,32] indicated that the hollow structure of the porous scaffold disappeared due to the filling of alloy into the struts for the composite. There are two main reasons responsible for the resultant compact microstructure: 1) the wettability between *β*-TCP and the Zn was good [38], which reduced infiltration resistance, and 2) both the gravity of Zn−Mg alloy and the external pressure exerted during the process of infiltration and solidification accelerated infiltration effectively.

The (*β*-TCP+MgO)/Zn−Mg composite showed a great improvement in the strength in comparison with the original porous *β*-TCP+MgO scaffold. The well-

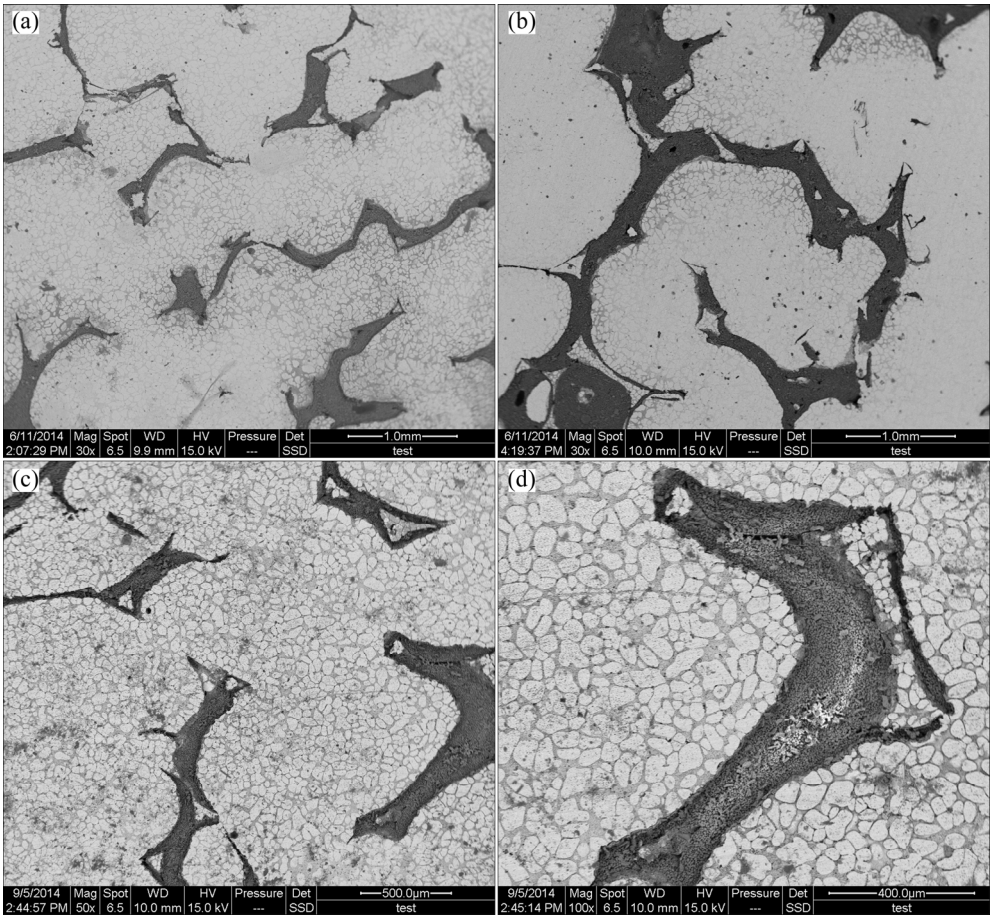

Fig. 9 Morphologies of (β-TCP+MgO)/Zn−Mg composite after 3 (a), 15 (b) and 30 d (c, d) of immersion in SBF solution

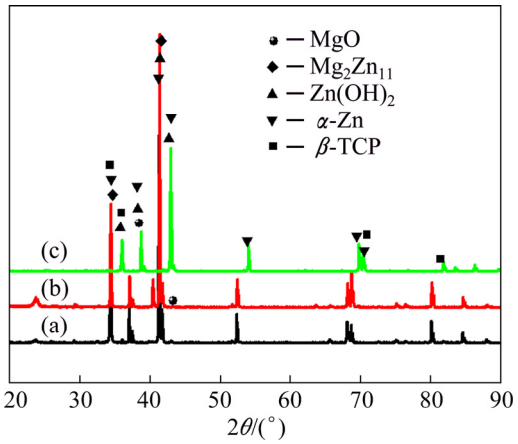

Fig. 10 XRD patterns of (β-TCP+MgO)/Zn−Mg composite after 3 (a), 15 (b) and 30 d (c) of immersion in SBF solution

improved mechanical behavior of the composite with interpenetrating networks may be attributed to the following reasons: 1) the excellent interlocking structure; 2) the strengthening and toughening effects of the matrix alloy, and 3) the crack closure force of the matrix alloy. This force may exert through bridging mechanism when external stress is applied and can hinder cracks initiation and growing effectively [31]. The interpenetration of the metal stabilizes the porous ceramic struts and partially prevents strut bending, resulting in a major improvement of the mechanical properties of the porous scaffold. On the other hand, the component phases of the composite forming an excellent interlocking structure stiffen the interface between matrix and reinforcement, which will result in the well-improved mechanical properties of the composite [39−41]. When load transferred from the infiltrated alloy to ceramic skeleton, crack would occur between the infiltrated metal and the ceramic skeleton during the compression process, so compared to the bulk alloy, the co-continuous composite often presented reduced mechanical property [40]. Meanwhile, crack propagated preferentially through the brittle ceramic phase, when it encountered the ductile metal, the metal deformed and the crack was bridged by the metal [42]. Many factors affect the compressive strength of the composite, such as compactness, the interfacial combination of matrix alloy and reinforcement, volume fraction and distribution uniformity of the reinforcement. Among these factors, the compactness and the interfacial combination have the greatest impact on the compressive property of the fabricated composites. Good metal−ceramic interfacial combination, metal bridging through plastic deformation and the crack deflection are the main reasons for the high strength [42]. For the resultant

(*β*-TCP+MgO)/Zn−Mg composite, the interfacial combination was good (as shown in Fig. 2(b)), the hollow structure of *β*-TCP+MgO scaffold has been filled by Zn−Mg alloy (as shown in Fig. 3(a)), but the intercontinuous brittle *β*-TCP+MgO led to the reduction in mechanical properties compared with Zn−Mg bulk alloy. Therefore, the mechanical properties of the co-continuous composite were between the properties of the porous ceramic and the metal [39].

Furthermore, the compressive strength of the (*β*-TCP+MgO)/Zn−Mg composite is also very close to that of the natural bone (2−180 MPa). Table 1 summarizes the ultimate compressive strength of different porous biomaterials, Zn alloy and composites. It should be noted that the reported alloys including the Mg−Zn, Mg−Ca and Zn demonstrated much higher compressive strength than the natural bone. However, some other porous materials such as porous Mg and porous polymers were too lower to be suitable for natural bone. In comparison, the mechanical properties of co-continuous Zn−Mg composites can be adjusted by adding suitable content of the *β*-TCP+MgO and satisfy the requirement of implant bone materials.

Table 1 Ultimate compressive strength of different biomaterials in comparison to natural bone

Material	Porosity/%	Pore size/μm	Compressive strength/MPa	Ref.
Porous Mg	36−55	200−400	15−31	[27]
Porous polymers	58−80	~300	2.7−11	[27]
Porous HA	50−77	200−400	12−17.4	[27]
Porous *β*-TCP	73±0.4	300−400	~2.9	[43]
Mg−Zn	−	−	433.7±1.4	[44]
Mg−1Ca	−	−	240	[45]
Zn−1Mg−1Ca alloy	−	−	300	[46]
Co-continuous *β*-TCP/MgCa composite	−	−	147±13	[32]
Interpenetrating *β*-TCP/Mg−Zn−Mn composite	−	−	140±20	[31]
Natural bone	−	−	2−180	[27]

For bone implantation, the (*β*-TCP+MgO)/Zn−Mg composite with improved mechanical strength will promote its load capacity when it is implanted into the bone. After periods of implantation, Zn−Mg will be degraded gradually and pores will be left onsite, which will improve the ingrowth of bone tissue. From the immersion experimental results, it is reasonable to deduce that shortly after the implantation in the bone, the bone tissue will grow towards the degradation of Zn−Mg matrix alloy while the remaining *β*-TCP+MgO networks still maintain their geometrical shape and carry the physiological load for the tissue ingrowth [29].

In general, (*β*-TCP+MgO)/Zn−Mg composite had better corrosion resistance than Zn−Mg bulk alloy. Compared with Zn−Mg bulk alloy after different immersion time, the greatest distinction of the morphologies for the resultant composite might be the existence of *β*-TCP+MgO scaffold. It can be seen from Figs. 9(c) and (d) that, slight crevice corrosion exists along the interface between Zn−Mg matrix alloy and the scaffold. In our previous study, crevice corrosion also exists along the interfaces between MgCa alloy and the HA+*β*-TCP scaffolds, between Mg−Zn−Mn alloy and *β*-TCP scaffold, and compared with other composites, the worse interface combination of (85HA+*β*-TCP)/MgCa and HA/MgCa composites resulted in more serious crevice corrosion [31,45]. The ceramic/metal interface has the capability of forming a galvanic couple in the electrolyte and the electrically conducting scaffold becomes the noble member. The corrosion initiated along the interface, allowing the electrolyte deep penetration [47,48]. As the corrosion proceeds, the Zn−Mg matrix alloy dissolves gradually with *β*-TCP+MgO scaffold structure left, as shown in Figs. 9(c) and (d). With time extending, the corrosion reactions continue along the interface between the metal matrix and ceramic, swelling the composite and allowing the electrolyte to penetrate more deeply till the composite completely breaks down [48].

The influence of Mg on the corrosion rate and corrosion parameters of the Zn−Mg alloys is small. Moreover, Mg forms the Mg_2Zn_{11} phase in the Zn−Mg alloys, but the standard potential of this phase is not very different from that of pure zinc. Therefore, the formation of galvanic micro-cells between Zn and Mg_2Zn_{11}, which would accelerate corrosion and shift the corrosion parameters, is unlikely [16]. But when Zn is exposed to the SBF solution, Zn in aqueous solution dissolves according to the following equations [49]:

Anodic reaction:

$$Zn(s) \rightarrow Zn^{2+}(aq)+2e \quad (1)$$

Cathodic reaction:

$$2H_2O(l)+2e \rightarrow H_2(g)+2OH^- (aq) \quad (2)$$

Product formation:

$$Zn^{2+}(aq)+2OH^-(aq) \rightarrow Zn(OH)_2(s) \quad (3)$$

$$Zn(OH)_2+4Zn^{2+}+2Cl^-+6OH^- \rightarrow Zn_5(OH)_8Cl_2 \quad (4)$$

Thus, $Zn(OH)_2$ protective film formed firstly on the surface of the (*β*-TCP+MgO)/Zn−Mg composite during the immersion period. Then, the chloride ions (Cl^-) of the SBF solution would react with $Zn(OH)_2$ to form a

resoluble $Zn_5(OH)_8Cl_2$, so that the protective film was destroyed, which made the deep fresh Zn−Mg alloy substrate expose to the solution. In this way, the formation and the damage of the $Zn(OH)_2$ film would cycle until the Zn−Mg alloy was completely exhausted. WITTE et al [50] also reported that occasionally localized corrosion of AZ91D−HA composite was interrupted as a breakdown and reformation of the protective surface layer. Mg-rich phase was corroded firstly to form Mg-based oxide, hydroxide or carbonate. These Mg-containing corrosion products acted as semiconductors and formed a protective layer on the exposed surface. This protective layer separated the corrosive environment with the metal and contributed to a general precipitation of Mg-modified simonkolleite, which may inhibit localized corrosion [36]. As can be observed in Fig. 7, the pH value of SBF solution incubating the composite increased in the early immersion period because of the dissolution of Zn−Mg and the releasing of hydroxide ions (OH^-) into the solution near the surface (Eqs. (1) and (2)). Afterwards, the increase in pH of SBF adjacent to the surface of the sample disturbed the anodic reaction (Eq. (1)) and suppressed the production of Zn^{2+}. At the same time, the formation of protective $Zn(OH)_2$ layer (Eq. (3)) on the surface of the sample would restrict the diffusion of all ions in the solution and retard the degradation. LIU et al [51] also found that the addition of β-TCP particles could result in the formation of a passive surface film, which enhanced the corrosion resistance of Mg−1Ca−2Zn alloy. But the reaction of the (β-TCP+MgO)/Zn−Mg composite was significantly slow, as it only caused the pH value to increase to approximately 7.8 after 1 d of immersion, and then the dissolution of $Zn(OH)_2$ consumed the OH^- of the SBF solution and the pH value decreased slowly. When the reactions among all the ions got equilibrium, the pH value of the SBF solution kept at a relatively stable level of about 7.3 (as shown in Fig. 7).

With the increase of immersion time, Zn^{2+} concentration in the SBF is determined by the three processes as follows: 1) the increase in the concentration of Zn^{2+} due to the dissolution of Zn−Mg alloy through Eq. (1); 2) the decrease in the Zn^{2+} concentration due to the formation of protective $Zn(OH)_2$ layer, which consumes Zn^{2+} through Eq. (3) and restricts the dissolusion of Zn into the SBF; 3) the dissolution of the protective $Zn(OH)_2$ layer. $Zn(OH)_2$ is attracted by chloride ions (Cl^-) in the solution to form a more resoluble $Zn_5(OH)_8Cl_2$, so the $Zn(OH)_2$ layer is loose and its dissolution makes the surface more active, subsequently this decreases the protected area and causes the further dissolution of Zn−Mg alloy and the increase in the Zn^{2+} concentration. The compensative effect made the Zn^{2+} concentrations for the bulk alloy and the composite increase with the increase of immersion time (as shown in Fig. 8).

Compared with the Zn−Mg alloy and porous β-TCP and other biomedical composites [16,52−54], the mechanical properties and corrosion behaviors of the co-continuous (β-TCP+MgO)/Zn−Mg composite can satisfy the requirement of implant materials. When the Zn−Mg alloy was infiltrated into the porous β-TCP+MgO, its mechanical properties would be greatly improved due to the compact structure and the good interfacial combination. Meanwhile, Zn−Mg matrix alloy and β-TCP+MgO have different biodegradation rates, thus the co-continuous (β-TCP+MgO)/Zn−Mg composite can be designed to own adjustable biodegradation and osteoconduction properties by changing the ratio of the β-TCP+MgO and Zn−Mg. So, this composite is a very promising candidate for bone substitute.

5 Conclusions

1) The co-continuous (β-TCP+MgO)/Zn−Mg composite for biodegradable bone implant material was fabricated using suction exsorption technique. The resultant composite had compact microstructure and the interconnected network structure was evident.

2) The ultimate compressive strength of the (β-TCP+MgO)/Zn−Mg composite was 244 MPa, which was about 1000 times higher than that of the original porous scaffold and 2/3 of the strength of the Zn−Mg bulk alloy.

3) The electrochemical and immersion test both indicated that the corrosion resistance of the (β-TCP+MgO)/Zn−Mg composite was better than that of the Zn−Mg bulk alloy. Additionally, the immersion test also indicated that the β-TCP+MgO scaffold was left behind due to its much slower degradation rate than that of the Zn−Mg matrix alloy for the (β-TCP+MgO)/Zn−Mg composite. The corrosion products on the composite surface were mainly $Zn(OH)_2$.

4) Appropriate mechanical and corrosion properties of the (β-TCP+MgO)/Zn−Mg composite indicate the possibility for new biomaterials.

References

[1] TAN Li-li, YU Xiao-ming, WAN Peng, YANG Ke. Biodegradable materials for bone repairs: A review [J]. Journal of Materials Science and Technology, 2013, 29: 503−513.

[2] ZIGNANI M, MINH T L, EINMAHL S, TABATABAY C, HELLER J, ANDERSON J M, GURNY R. Improved biocompatibility of a viscous bioerodible poly(ortho ester) by controlling the environmental pH during degradation [J]. Biomaterials, 2000, 21: 1773−1778.

[3] BOSE S, TARAFDER S. Calcium phosphate ceramic systems in growth factor and drug delivery for bone tissue engineering: A review [J]. Acta Biomaterialia, 2012, 8: 1401−1421.

[4] ZHANG X, TAKAHASHI T, VECCHIO K S. Development of bioresorbable Mg-substituted tricalcium phosphate scaffolds for bone tissue engineering [J]. Materials Science and Engineering C, 2009, 29: 2003−2010.

[5] DU Hui, WEI Zun-jie, WANG Hong-wei, ZHANG Er-lin, ZUO Lin, DU Lian-ping. Surface microstructure and cell compatibility of calcium silicate and calcium phosphate composite coatings on Mg−Zn−Mn−Ca alloys for biomedical application [J]. Colloids and Surfaces B, 2011, 83: 96−102.

[6] WU Rui-zhi, YAN Yong-de, WANG Gui-xiang, MURR L E, HAN Wei, ZHANG Zhong-wu, ZHANG Mi-lin. Recent progress in magnesium−lithium alloys [J]. International Materials Reviews, 2015, 60: 65−100.

[7] REIFENRATH J, KRAUSE A, BORMANN D, RECHENBERG B V, WINDHAGEN H, MEYER-LINDENBERG A M. Profound differences in the in-vivo-degradation and biocompatibility of two very similar rare-earth containing Mg-alloys in a rabbit model [J]. Materials Science and Engineering, 2010, 41: 1054−1061.

[8] BAKHSHESHI-RAD H R, IDRIS M H, ABDUL-KADIR M R, OURDJINI A, MEDRAJ M, DAROONPARVAR M, HAMZAH E. Mechanical and bio-corrosion properties of quaternary Mg−Ca−Mn−Zn alloys compared with binary Mg−Ca alloys [J]. Materials and Design, 2014, 53: 283−292.

[9] ZHANG Shao-xiang, ZHANG Xiao-nong, ZHAO Chang-li, LI Jia-nan, SONG Yang, XIE Chao-Ying, TAO Hai-rong, ZHANG Yan, HE Yao-hua, JIANG Yao, BIAN Yu-jun. Research on an Mg−Zn alloy as a degradable biomaterial [J]. Acta Biomaterialia, 2010, 6: 626−640.

[10] YIN Dong-song, ZHANG Er-lin, ZENG Song-yan. Effect of Zn on mechanical property and corrosion property of extruded Mg−Zn−Mn alloy [J]. Transactions of Nonferrous Metals Society of China, 2008, 18: 763−768.

[11] PENG Q M, HUANG Y D, ZHOU L, HORT N, KAINER K U. Preparation and properties of high purity Mg−Y biomaterials [J]. Biomaterials, 2010, 31: 398−403.

[12] WITTE F, KAESE V, HAFERKAMP H, SWITZER E, MEYER-LINDENBERG A, WIRTH C J, WINDHAGEN H. In vivo corrosion of four magnesium alloys and the associated bone response [J]. Biomaterials, 2005, 26: 3557−3563.

[13] ZHANG Er-lin, YANG Lei. Microstructure, mechanical properties and bio-corrosion properties of Mg−Zn−Mn−Ca alloy for biomedical application [J]. Materials Science and Engineering A, 2008, 497: 111−118.

[14] SONG G L, HAPUGODA S, JOHN D S. Degradation of the surface appearance of magnesium and its alloys in simulated atmospheric environments [J]. Corrosion Science, 2007, 49: 1245−1265.

[15] VOJTĚCH D, KUBÁSEK J, ŠERÁK J, NOVÁK P. Mechanical and corrosion properties of newly developed biodegradable Zn-based alloys for bone fixation [J]. Acta Biomaterialia, 2011, 7: 3515−3522.

[16] LUO X M, BARBIERI D, DAVISON N, YAN Y G, BRUIJN J D, YUAN H P. Zinc in calcium phosphate mediates bone induction: In vitro and in vivo model [J]. Acta Biomaterialia, 2014, 10: 477−485.

[17] MOONGA B S, DEMPSTER D W. Zinc is a potent inhibitor of osteoclastic bone resorption in vitro [J]. Journal of Bone and Mineral Research, 1995, 10: 453−457.

[18] LAKHKAR N J, LEE I H, KIM H W, SALIH V, WALL I B, KNOWLES J C. Bone formation controlled by biologically relevant inorganic ions: Role and controlled delivery from phosphate-based glasses [J]. Advanced Drug Delivery Reviews, 2013, 65: 405−420.

[19] KALIČANIN B M, NIKOLIĆ R S. Potentiometric stripping analysis of zinc and copper in human teeth and dental materials [J]. Journal of Trace Elements in Medicine and Biology, 2008, 22: 93−99.

[20] MIAO Shun-dong, CHENG Kui, WENG Wen-jian, DU Pi-yi, SHEN Ge, HAN Gao-rong, YAN Wei-qi, ZHANG San. Fabrication and evaluation of Zn containing fluoridated hydroxyapatite layer with Zn release ability [J]. Acta Biomaterialia, 2008, 4: 441−446.

[21] ZOU Yuan-wen, HUANG Zhong-bing, DENG Min, YIN Guang-fu, CHEN Xian-chun, LIU Juan, WANG Yan, YAN Li, GU Jian-wen. Synthesis and neuro-cytocompatibility of magnetic Zn−ferrite nanorods via peptide-assisted process [J]. Journal of Colloid and Interface Science, 2013, 408: 6−12.

[22] ONOKI T, YAMAMOTO S, ONODERA H, NAKAHIRA A. New technique for bonding hydroxyapatite ceramics and magnesium alloy by hydrothermal hot-pressing method [J]. Materials Science and Engineering C, 2011, 31: 499−502.

[23] KWON S H, JUN Y K, HONG S H, KIM H E. Synthesis and dissolution behavior of β-TCP and HA/β-TCP composite powders [J]. Journal of the European Ceramic Society, 2003, 23: 1039−1045.

[24] FENG Ai-ling, HAN Yong. Mechanical and in vitro degradation behavior of ultrafine calcium polyphosphate reinforced magnesium-alloy composites [J]. Materials and Design, 2011, 32: 2813−2820.

[25] SALMA-ANCANE K, STIPNIECE L, PUTNINS A, BERZINA-CIMDINA L. Development of Mg-containing porous β-tricalcium phosphate scaffolds for bone repair [J]. Ceramics International, 2015, 41: 4996−5004.

[26] NIKAIDO T, TSURU K, MUNAR M, MARUTA M, MATSUYA S, NAKAMURA S, ISHIKAWA K. Fabrication of β-TCP foam: Effects of magnesium oxide as phase stabilizer on its properties [J]. Ceramics International, 2015, 41: 14245−14250.

[27] CORBIN S F, ZHAO J X, HENEIN H, APTE P S. Functionally graded metal/ceramic composites by tape casting, lamination and infiltration [J]. Materials Science and Engineering A, 1999, 262: 192−203.

[28] SON J H, LEE W J, PARK Y H, PARK I M. Fabrication and thermal expansion behavior of a magnesium−matrix composite with a high content of reinforcing SiC particles [J]. Mechanics of Composite Materials, 2011, 47: 427−434.

[29] MIAO X, LIM W K, HUANG X, CHEN Y. Preparation and characterization of interpenetrating phased TCP/HA/PLGA composites [J]. Materials Letters, 2005, 59: 4000−4005.

[30] WANG Xiang, LI Jing-tao, XIE Ming-yu**,** QU Li-jie, ZHANG Peng, LI Xin-lin. Structure, mechanical property and corrosion behaviors of (HA+β-TCP)/Mg−5Sn composite with interpenetrating networks [J]. Materials Science and Engineering C, 2015, 56: 386−392.

[31] WANG Xiang, ZHANG Peng, DONG Li-hua, MA Xu-liang, LI Jing-tao, ZHENG Yu-feng. Microstructure and characteristics of interpenetrating β-TCP/Mg−Zn−Mn composite fabricated by suction casting [J]. Materials and Design, 2014, 54: 995−1001.

[32] MA Xu-liang, DONG Li-hua, WANG Xiang. Microstructure, mechanical property and corrosion behavior of co-continuous β-TCP/MgCa composite manufactured by suction casting [J]. Materials and Design, 2014, 56(4): 305−312.

[33] MIAO X G, TAN D M F, LI J, XIAO Y, CRAWFORD R. Mechanical and biological properties of hydroxyapatite/tricalcium phosphate scaffolds coated with poly(lactic-co-glycolic acid) [J]. Acta Biomaterialia, 2008, 4: 638−645.

[34] WANG Xiang, DONG Li-hua, MA Xu-liang, ZHENG Yu-feng. Microstructure, mechanical property and corrosion behaviors of interpenetrating C/Mg−Zn−Mn composite fabricated by suction casting [J]. Materials Science and Engineering C, 2013, 33: 618−625.

[35] ASTM−G31−72. Standard practice for laboratory immersion corrosion testing of metals [S]. ASTM 2004.

[36] YAO C Z, WANG Z C, TAY S L, ZHU T P, GAO W. Effects of Mg on microstructure and corrosion properties of Zn−Mg alloy [J]. Journal of Alloys and Compounds, 2014, 602: 101−107.

[37] TAPIERO H, TEW K D. Trace elements in human physiology and pathology: Zinc and metallothioneins [J]. Biomedicine and Pharmacotherapy, 2003, 57: 399−411.

[38] PINA S, VIEIRA S I, TORRES P M C, GOETZ-NEUNHOEFFER F, NEUBAUER J, da CRUZ E SILVA O A B, da CRUZ E SILVA E F, FERREIRA J M F. In vitro performance assessment of new brushite-forming Zn- and ZnSr-substituted β-TCP bone cements [J]. Journal of Biomedical Materials Research: Part B, 2010, 94: 414−420.

[39] LU Yuan, YANG Jian-feng, LU Wei-zhong, LIU Rong-zhen, QIAO Guan-juan, BAO Chong-gao. The mechanical properties of co-continuous Si_3N_4/Al composites manufactured by squeeze casting [J]. Materials Science and Engineering A, 2010, 527: 6289−6299.

[40] ZESCHKY J, LO J, HÖFNER T, GREIL P. Mg alloy infiltrated Si−O−C ceramic foams [J]. Materials Science and Engineering A, 2005, 403: 215−221.

[41] ZHANG D, XIE X Q, FAN T X, SUN B H, SAKATA T, MORI H, OKABE T. Microstructure and properties of ecoceramics/metal composites with interpenetrating networks [J]. Materials Science and Engineering A, 2003, 351: 109−116.

[42] CHANG H, HIGGINSON R, BINNER J. Microstructure and property characterisation of 3-3 Al(Mg)/Al_2O_3 interpenetrating composites produced by a pressureless infiltration technique [J]. Journal of Materials Science, 2010, 45: 662−668.

[43] RAMAY H R R, ZHANG M. Biphasic calcium phosphate nanocomposite porous scaffolds for load-bearing bone tissue engineering [J]. Biomaterials, 2004, 25: 5171−5180.

[44] ZIOUPOS P, COOK R B, HUTCHINSON J R. Some basic relationships between density values in cancellous and cortical bone [J]. Journal of Biomechanics, 2008, 41: 1961−1968.

[45] WANG Xiang, DONG Li-hua, LI Jing-tao, LI Xin-lin, MA Xu-liang, ZHENG Yu-feng. Microstructure, mechanical property and corrosion behavior of interpenetrating (HA+β-TCP)/MgCa composite fabricated by suction casting [J]. Materials Science and Engineering C, 2013, 33: 4266−4273.

[46] LI Hua-fang, YANG Hong-tao, ZHENG Yu-feng, ZHOU Fei-yu, QIU Ke-jin, WANG Xiang. Design and characterizations of novel biodegradable ternary Zn-based alloys with IIA nutrient alloying elements Mg, Ca and Sr [J]. Materials and Design, 2015, 83: 95−102.

[47] GU X N, WANG X, LI N, LI L, ZHENG Y F, MIAO X G. Microstructure and characteristics of the metal-ceramic composite (MgCa-HA/TCP) fabricated by liquid metal infiltration [J]. Journal of Biomedical Materials Research: Part B, 2011, 99: 127−134.

[48] RAZAVI M, FATHI M H, MERATIAN M. Microstructure, mechanical properties and bio-corrosion evaluation of biodegradable AZ91-FA nanocomposites for biomedical applications [J]. Materials Science and Engineering A, 2010, 527: 6938−6944.

[49] SHI Yan-yan, ZHANG Zhao, ZHANG Jian-qing, CAO Chu-nan. Review of atmospheric corrosion of zinc and zinc alloy [J]. Journal of Chinese Society for Corrosion and Protection, 2005, 25: 373−379. (in Chinese)

[50] WITTE F, FEYERABEND F, MAIER P, FISCHER J, STÖRMER M, BLAWERT C, DIETZEL W, HORT N. Biodegradable magnesium-hydroxyapatite metal matrix composites [J]. Biomaterials, 2007, 28: 2163−2174.

[51] LIU D B, HUANG Y, PRANGNELL P B. Microstructure and performance of a biodegradable Mg−1Ca−2Zn−1TCP composite fabricated by combined solidification and deformation processing [J]. Materials Letters, 2012, 82: 7−9.

[52] KOC N, TIMUCIN M, KORKUSUZ F. Fabrication and characterization of porous tricalcium phosphate ceramics [J]. Ceramics International, 2004, 30: 205−211.

[53] SÁNCHEZ-SALCEDO S, BALAS F, IZQUIERDO-BARBA I, VALLET-REGÍ M. In vitro structural changes in porous HA/β-TCP scaffolds in simulated body fluid [J]. Acta Biomaterialia, 2009, 5: 2738−2751.

[54] RAZAVI M, FATHIM M H, MERATIAN M. Bio-corrosion behavior of magnesium−fluorapatite nanocomposite for biomedical applications [J]. Materials Letters, 2010, 64: 2487−2490.

真空吸渗法制备生物医用相互连续 (β-TCP+MgO)/Zn−Mg 复合材料的组织和性能

王 香[1]，聂其东[1]，马旭梁[2]，范金龙[1]，颜延亮[1]，李新林[1]

1. 哈尔滨工程大学 表界面科学与技术研究所，
教育部超轻材料与表面/界面技术重点实验室，哈尔滨 150001；
2. 哈尔滨理工大学 材料科学与工程学院，哈尔滨 150080

摘　要：利用真空吸渗技术通过将 Zn−Mg 合金渗透到多孔 β-TCP+MgO 中制备生物医用相互连续(β-TCP+MgO)/Zn−Mg 复合材料。采用扫描电镜(SEM)、X 射线衍射仪(XRD)、力学性能测试、电化学和浸泡实验研究复合材料的显微组织、力学性能和腐蚀行为。研究结果表明，熔融 Zn−Mg 合金不仅渗入到多孔 β-TCP+MgO 骨架的孔隙中，也渗入到筋中，形成致密的复合材料。Zn−Mg 合金与 β-TCP+MgO 骨架接触紧密，在合金与骨架之间没有发现反应层。复合材料的压缩强度达 244 MPa，为原始多孔 β-TCP+MgO 骨架强度的 1000 倍以上，相当于 Zn−Mg 大块合金强度的 2/3。在模拟体液中的电化学和浸泡测试结果表明，复合材料的耐腐蚀性优于 Zn−Mg 大块合金的。复合材料表面的腐蚀产物主要是 $Zn(OH)_2$。合适的力学性能和腐蚀性能表明真空吸渗法制备的(β-TCP+MgO)/Zn−Mg 复合材料将是潜在的骨替代材料。

关键词：(β-TCP+MgO)/Zn−Mg 复合材料；显微组织；力学性能；腐蚀行为；真空吸渗

(Edited by Wei-ping CHEN)